This full text paper was peer reviewed at the direction of IEEE Communications Society subject matter experts for publication in the IEEE INFOCOM 2008 proceedings.

The Meandering Current Mobility Model and its Impact on Underwater Mobile Sensor Networks

*Antonio Caruso, *Francesco Paparella, †Luiz F. M. Vieira, ‡Melike Erol, †Mario Gerla

*Mathematics Department, University of Salento, Lecce, Italia
†UCLA Computer Science Department, Los Angeles, California
‡Istanbul Technical University, Computer Engineering Department, Istanbul, Turkey

{antonio.caruso,francesco.paparella}@unile.it, {luiz, erol, gerla}@cs.ucla.edu

***Abstract*—Underwater mobile acoustic sensor networks are promising tools for the exploration of the oceans. These networks require new robust solutions for fundamental issues such as: localization service for data tagging and networking protocols for communication. All these tasks are closely related with connectivity, coverage and deployment of the network. A realistic mobility model that can capture the physical movement of the sensor nodes with ocean currents gives better understanding on the above problems. In this paper, we propose a novel physically-inspired mobility model which is representative of underwater environments. We study how the model affects a range-based localization protocol, and its impact on the coverage and connectivity of the network under different deployment scenarios.**

I. Introduction

Sensor networks represent a new remote monitoring and control technology, and recently, have become a promising technology for underwater environment monitoring.

The idea of applying sensor networks into underwater environments, forming underwater sensor networks (UWSN) started an exciting research area, attracting a growing interest from the network community. These networks are envisioned to enable new applications including: military underwater surveillance, oceanographic data collection, ecology (e.g. pollution, water quality and biological monitoring), public safety (e.g. disaster prevention, seismic and tsunami monitoring), industrial (offshore exploration).

Recent works have addressed some of the challenges presented by underwater sensors [1]–[3]. Since UWSN is an emerging topic, up to now, most of the researches have mainly focused on fundamental sensor networking problems such as data gathering [4], synchronization [5], localization [6], routing protocols [7], [8], energy minimization and MAC [9], [10] issues. Various architectures have been proposed for UWSN, they can be classified in the following groups: i) ocean floor embedded sensor networks [1], ii) UWSNs with sensors attached either to anchors on the ocean floor [1] or to surface moorings [11], iii) hybrid architectures [12] iv) Autonomous Underwater Vehicle (AUV) aided UWSNs where AUVs are used for additional support in any of the above architectures [13] v) networks with free-floating sensors (mobile underwater sensor networks) [14].

Currently, only sensors without networking capability are widely used in oceanographic research. These sensors are used in two distinct and complementary ways to perform measurements in the oceans; Eulerian and Lagrangian. In the Eulerian approach data are taken at positions that do not change in time (e.g. from a mooring or from a ship standing still with respect to the bottom). In the Lagrangian approach, data are taken from autonomous devices that passively follow the ocean currents, for a review see [15]. Lagrangian autonomous devices (usually named *floats* or *drifters*) give unique insights into the structure and patterns of ocean flows, at many different temporal and spatial scales. An operational forerunner of future global arrays of lagrangian devices is the Argo project: a set of thousands of free-drifting profiling floats that measure temperature, salinity, and velocity of the ocean water [16].

Although the devices in use today are not able to communicate with each other, there is a growing trend of using lagrangian devices for monitoring regional and coastal areas [17]. In those settings the small distance between the devices makes it possible to acoustically interconnect them and deploy them as underwater mobile acoustic sensor networks.

Terrestrial sensor networks generally assume fairly dense deployment with continuously connected coverage of an area using inexpensive, stationary nodes. In contrast with this, economics push underwater networks toward sparse and mobile deployments. A recent survey [2] on underwater networks highlights the importance of *sparse* and *mobile* networks due to the immense volume of the underwater domain.

In this paper, we study underwater mobile acoustic sensor networks that consist of free-floating sensors with networking capability. We present a mobility model for underwater environments, the *Meandering Current Mobility model* (MCM hereafter). This model considers sensors moving by the effect of meandering sub-surface currents and vortices. The domain model is representative of a large coastal environment. Therefore, unlike previous works, we assume a domain spanning several kilometers. In this case, deployment of the network with sensors uniformly distributed over this large domain would be unrealistic. Instead, we consider an initial deployment of nodes in a small subarea where they are

978-1-4244-2026-1/08/$25.00 © 2008 IEEE

Authorized licensed use limited to: UNIVERSITY OF LECCE. Downloaded on February 27,2010 at 15:07:02 EST from IEEE Xplore. Restrictions apply.

released and thereafter move according to the mobility model. This scenario is more realistic for underwater mobile sensor networks applications, especially in monitoring the dynamics of the oceans.

For any sensor network, the *lifetime* of the network is usually defined as a set of application specific requirements: the connectivity among nodes, the coverage of the network, i.e. the fraction of the area where sensors can effectively collect information and on the performances of network protocols. In a mobile network connectivity and coverage vary when the nodes move. Hence studying these metrics with a realistic mobility model is essential. The performance of any protocol is directly related with these issues. We study the dynamic coverage and connectivity as a function of time under the MCM model. We also consider the effect of different deployment strategies on network coverage and connectivity.

Underwater sensor networks, like other sensor networks, require a *localization service* in order to geo-reference each measurement. We present a localization service, tailored to the specifics of underwater sensor network, and study the effect of the mobility model on the level of service provided by the localization protocol.

The paper is organized as follows: In Section II, we define a mobility model from oceanography that provides a good degree of accuracy in modeling coastal deep water ocean currents. In Section III, we present the network model, the deployment process, the connectivity and coverage metrics. In Section IV, we present the localization scheme. In Section V we present the simulation outcomes and discuss the impact of the mobility model on the connectivity, coverage and localization using different deployment schemes. Section VI draws the main conclusions and possible future works.

II. Mobility Model

In order to study the networking properties of interconnected sensors, it is crucial to use a mobility model that takes into account the fluid nature of the medium in which they move. Almost all models in the existing literature on mobile sensor networks assume that each sensor moves independently from the others [18]–[20]. Typically, the path of each sensor is taken as an independent realization of a given stochastic process, such as a random walk, or a random way point process. In a fluid, instead, the same velocity field advects all the sensors. Their paths are deterministic (albeit often chaotic), and strong correlations between nearby sensors must be expected. Then, in order to simulate the movement of sensors, one needs to model the movement of the ocean in which they are immersed. This may be achieved in several ways, with varying levels of realism.

On one hand, the latest advances in computational techniques allow for very realistic but complex "ocean forecasts", similar to weather forecasts [21]; this approach, in addition to the sheer computational cost of the simulation, requires additional detailed knowledge of atmospheric forcing, bottom topography and boundary conditions, which comes from extensive field observations.

On the other hand, progress in the understanding of lagrangian transport have been made with a purely kinematic approach, where a (reasonable) velocity field is prescribed beforehand. For our applications, we exploit the fact that the oceans are a stratified, rotating fluid, hence vertical movements are, almost everywhere, negligible with respect to the horizontal ones [22]. Thus we will assume that our lagrangian sensors move on horizontal surfaces, and neglect their vertical displacements. Models of this sort are very well known in fluid dynamics, because they allow to describe the kinematics of quasi-two-dimensional flows in a simple way, while retaining a good level of realism. The book [23] is a general introduction for the interested reader, while the very recent monograph [24] focuses on geophysical applications.

In oceanography, the absence of vertical movements is a design feature of *drifters*, where the sensors hang at a fixed (small) depth under a buoyant object floating at the surface [25], [26]. In the case of *floats*, the operating depths are usually much larger, and there is no direct contact with the surface. The hull of the device is built in such a way to maintain its density almost constant, so that the float can be calibrated to follow a precisely defined isopycnal surface[1]; in this case, vertical movements of the float are usually limited to damped oscillations around the reference density surface triggered by internal waves [27].

Of course, in the presence of strong wind–driven upwelling or downwelling, or during events of deep water formation, or at the passage of exceptionally intense internal waves, the assumption of negligible vertical motions ceases to be valid. In our preliminary investigation, we feel appropriate to skip these exceptional events and propose a model that mimics conditions of ordinary water circulation.

Any incompressible, two-dimensional flow is described by a streamfunction ψ from which the two components of the divergenceless velocity field $\mathbf{u} \equiv (u, v)$ may be computed as:

$$u = -\frac{\partial \psi}{\partial y}; \quad v = \frac{\partial \psi}{\partial x}. \tag{1}$$

By a long-standing convention, u is the zonal (eastward) component of the velocity field and v is the meridional (northward) one. Then, the trajectory of a lagrangian device that moves with the current is the solution of the following system of Hamiltonian ordinary differential equations.

$$\dot{x} = -\partial_y \psi(x, y, t), \qquad \dot{y} = \partial_x \psi(x, y, t). \tag{2}$$

A widely studied streamfunction, which is designed to catch the two main features of a typical ocean flow (currents and vortices) was first proposed by Bower [28], who used the model to explain the properties of the observed paths of isopycnal floats released in the Gulf Stream. Her model was generalized in [29]. The resulting dynamics proved to be so rich and interesting that these early works sparked a very large number of other studies (too large to be summarized here, see [24] for a review).

[1] A surface of constant density. Isopycnal surfaces in the ocean are usually very close to be horizontal.

Authorized licensed use limited to: UNIVERSITY OF LECCE. Downloaded on February 27,2010 at 15:07:02 EST from IEEE Xplore. Restrictions apply.

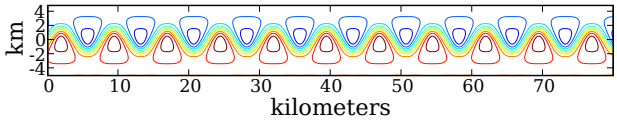

Fig. 1. A plot of the streamfunction (3) at $t = 0$, as seen in a reference frame moving with the phase speed c of the meanders. From eqn. (1) it follows that the velocity vectors are everywhere tangent to the streamfunction isolines, and their modulus is proportional to the modulus of the streamfunction gradient.

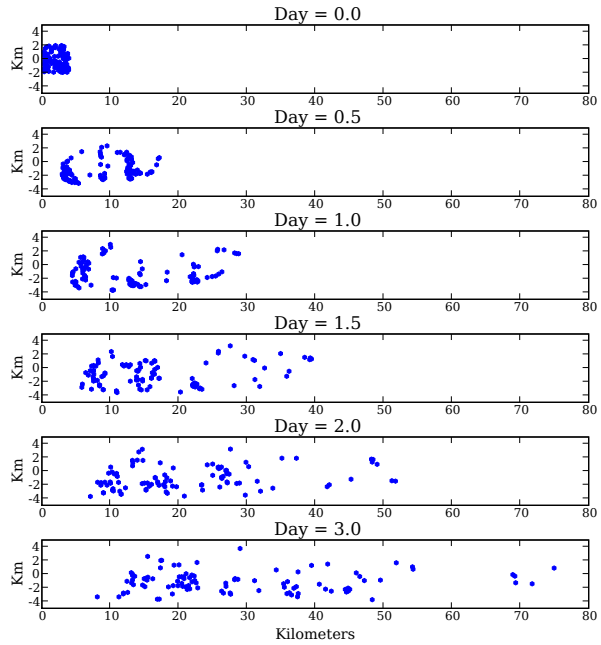

Fig. 2. Time evolution of the position of one hundred sensors randomly released in a square of 4 km of side centered on the axis of the jet-like current.

The non-dimensional form of the meandering jet model is

$$\psi(x, y, t) = -\tanh\left[\frac{y - B(t)\sin(k(x - ct))}{\sqrt{1 + k^2 B^2(t)\cos^2(k(x - ct))}}\right] \quad (3)$$

where $B(t) = A + \epsilon\cos(\omega t)$. This streamfunction represents a jet-like current, meandering between recirculating vortices (see Figure 1). The flow induces a net mass transport along the current, and, in a wide range of parameters, a vigorous chaotic mixing across the current.

In the expression (3) the parameter k sets the number of meanders in the unit length, c is the phase speed with which they shift downstream. The time–dependent function B modulates the width of the meanders: A determines the average meander width, ϵ is the amplitude of the modulation, and ω is its frequency. As a significant example, in the following we will use $A = 1.2$, $c = 0.12$, $k = 2\pi/7.5$, $\omega = 0.4$, $\epsilon = 0.3$. By taking one non-dimensional unit of space to be a kilometer, and one non-dimensional unit of time to be 0.03 days, we have that the size of the meanders is 7.5 km, the peak speed inside the jet is about 0.3 m/s, and the modulation period is about half a day (a value in agreement with the main tidal period). With these scalings we take the streamfunction in (3) as representative of a typical coastal current. The motion

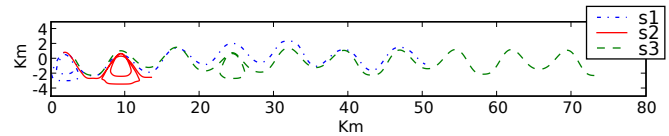

Fig. 3. Three representatives sensor trajectories as seen in a reference frame moving with speed c.

of lagrangian devices simulated by numerically integrating the equations (2) is shown in Figure 2.

For a thorough discussion on the choice of the parameters see [30] and references therein. Here we just observe that setting $\epsilon = 0$, and choosing a reference frame translating with speed c along the x axis, the streamfunction (3) becomes time–independent. For time–independent streamfunctions, a straightforward consequence of (2) is the fact that the motion of each sensor happens along the streamline[2] singled out by the initial condition. Because vortices are, by definition, regions of closed streamlines, it follows that sensors initially seeded inside the vortices will not be able to escape into the jet, and *vice-versa*. For $\epsilon \neq 0$ the streamfunction (3) is genuinely time–dependent: in no reference frame the sensor paths will coincide exactly with the streamlines. In this case there is some mass exchange between the vortices and the jet. Quantifying this exchange is not an easy matter: most of the literature cited above is devoted to just this problem. However, as a very rough rule of thumb, one should expect an increasing degree of permeability of the vortices as the parameter ϵ is increased.

Typical sensor paths (see Figure 3) show an alternation of fast downstream motion (when the sensor is in the jet) and looping motion (when the sensor is in a vortex). As a result, the trajectories of sensors trapped inside the same vortex remain strongly correlated, usually for several vortex turnovers. However, correlations are quickly lost when a sensor eventually leaves the vortex.

III. Network Model and Definitions

A mobile network is a time varying graph $G = (V(t), E(t))$ consisting of a large set $V(t)$ of sensor nodes moving in a rectangular domain at time t. The set $E(t)$ represents the communication link between sensors, i.e. $(u, v) \in E(t)$ if node u can send a packet to node v at time t. Set $E(t)$ is clearly time-dependent due to the variable channel conditions of the underwater environment and the effects of the mobility model. Successful reception of a transmission depends on the received signal strength, the interference caused by simultaneously transmitting nodes, and the ambient noise level. Moreover, shadowing, reflection, scattering and diffraction particularly affect acoustic underwater communications. We study homogeneous sensor networks, i.e. we assume that sensors transmit using the same power. We consider a transmitting power that result in a maximum communication range $R_c = 1000$m.

Usually, in the study of sensor networks, nodes are deployed in a small bounded geographic domain. Considering the spatial scale (kilometers) used by MCM we study nodes in a domain

[2]A streamline is a level curve of the streamfunction ψ.

Authorized licensed use limited to: UNIVERSITY OF LECCE. Downloaded on February 27,2010 at 15:07:02 EST from IEEE Xplore. Restrictions apply.

$D = [0, 80] \times [-4, 4]$ km. However, a physically acceptable model cannot confine the sensors inside an arbitrarily chosen domain. Our definition of the streamfunction implies that $\dot{y}$ approaches zero for large $|y|$: thus nodes follow the current oriented along the x-axis and eventually leave the domain through its right side (see Fig. 2). The set of nodes in the domain is therefore a function of the time.

Usually, works on sensor networks consider a single deployment of nodes, all at the same time instant, with uniform distribution (or using a Poisson process of a given intensity λ) over a small domain. We model the deployment of the network as a finite discrete random process: (N_i, D_i, T_i) with $0 \leq i < k$, where k is the number of deployment rounds, T_i is the time of the i-th deployment, N_i is the number of nodes deployed and D_i is the node distribution used to deploy the nodes. We consider it more realistic (and cost-effective) to deploy the nodes over a relatively small area of the domain: like a square $S = [0, 4] \times [-2, 2]$ km. In the following we assume that the distribution is uniform on S, i.e. $\forall\, i,\ D_i = U_S$ where U_S is equal to the uniform random distribution over S and zero outside S.

Consider a fixed number of sensors N. We study two simple versions of the above process: 1) the process $(N, U_S, 0)$ with $k = 1$ which models a single initial deployment of all nodes; and 2) the process $(N_0, U_S, i\Delta T)$ which models a k-phase deployments, where in each phase N_0 nodes are deployed at regular times. The constant quantity ΔT specifies the (waiting) time between two consecutive deployment rounds, the number of rounds k is equal to N/N_0[3]. The choice of the value of ΔT is of particular interest, its relation with the mobility model and its impact on the connectivity and coverage of the sensor networks is studied in Section V.

A. Measures for the analysis of the mobility model

To study sensors' advection, we introduce a measure from [31], called *absolute dispersion*. The absolute dispersion along the x-axis is defined as:

$$A^2(t, t_0) = \left\langle |x_i(t) - x_i(t_0)|^2 \right\rangle = \frac{1}{N} \sum_{i=1}^{N} |x_i(t) - x_i(t_0)|^2$$

where $N = |V|$ is the number of sensors in the network, $\langle \ldots \rangle$ indicates average over the sensor nodes, $x_i(t)$ is the x-coordinate of the $i-$th sensor at time t, t_0 is the time of deployment. We study the average of A^2 on different realizations of the same deployment process. The average of A^2 provides a network-wide measure for the dispersion of sensors as a function of time. The way the absolute dispersion scales with time characterizes the physical nature of the transport process: if $A^2 \propto t$ we are in the presence of a diffusive process; if $A^2 \propto t^2$ we have a ballistic transport process; if A^2 scales with a not integer power of time the underlying process is anomalously diffuse [31].

Note that, in a mobile underwater network, the combined effect of a limited transmit power, mobility over a large area, and limited communication ranges, implies that communications require multiple hops. Moreover, with high probability the communication graph G is partitioned in several connected components. To overcome this effect, routing techniques from disruption and delay tolerant networking (DTN) can be used [32]. For this reason the analysis of the dispersion of nodes belonging to the largest connected component (LCC) is of particular interest.

Denoting with $LCC(t)$ the set of sensors in the largest connected component at time t, we define the bounding box functions $x^{lcc}_{min}(t) = \min_{i \in LCC(t)} x_i(t)$ and $x^{lcc}_{max}(t) = \max_{i \in LCC(t)} x_i(t)$. We compare the bounding box of $LCC(t)$ with the bounding box of the whole network, i.e. $x^{G}_{min}(t) = \min_{i \in V(t)} x_i(t)$ and $x^{G}_{max}(t) = \max_{i \in V(t)} x_i(t)$.

B. Coverage and Connectivity

The *sensing area* is the area where a node can sense the environment or detect events, and it is modeled by a disk of radius R_s centered at the sensor position. We assume that each sensor node has the same sensing capability. A point of the domain is *covered* by a sensor if it is located in the sensing area of some sensor. For each static distribution of nodes, the domain can be partitioned in two areas: the covered region, which is the set of points covered by at least one sensor, and the uncovered region defined as the complement of the covered region. We use two measures, from [33], for static and mobile coverage:

Definition 3.1 (Area Coverage): The area coverage of a sensor network at time t, $f_a(t)$ is the fraction of the geographical area covered by one or more sensors at time t.

Definition 3.2 (Area Coverage over a time-interval): The area coverage of a mobile sensor network during the time interval $[0, t)$, $f_m(t)$ is the fraction of the geographical area covered by at least one sensor at some point of time within $[0, t)$.

The area coverage is important for applications that require simultaneous coverage of the geographic domain. The coverage $f_m(t)$ is more appropriate for applications that do not require simultaneous coverage of all points at specific time instants, but prefer to cover the network within some time interval.

IV. Localization

Most of the underwater sensor network applications require location information. This information is used in data tagging. Besides, once the location information is retrieved, it can be used in position-based routing algorithms.

Outdoor terrestrial sensor nodes can benefit from Global Positioning Service (GPS) whereas underwater sensor nodes need alternative solutions. GPS cannot be used underwater because the high frequency GPS signal does not propagate well through water. Localization without GPS is a challenging task. Though GPS-free localization have been studied for terrestrial sensor networks these results cannot be directly applied to UWSNs due to large amount of communication overhead or the required infrastructure.

[3]We chose N_0 a divisor of N in order to have k integer.

Authorized licensed use limited to: UNIVERSITY OF LECCE. Downloaded on February 27,2010 at 15:07:02 EST from IEEE Xplore. Restrictions apply.

There are several works on localization for UWSNs [34]–[36]. In this work, we consider a set of initial *beacons* such as "sound sources" or "Dive and Rise" [36] beacons that acquire and announce their coordinates. Sound sources are special devices placed in the ocean emitting signals which can travel thousands of kilometers. DNR nodes have the ability to move vertically, reach above the water to receive GPS coordinates and distribute the updated coordinates while they sink.

In both cases, a supplementary localization protocol, where the coordinates of the first set of beacons are exchanged among nodes, would be helpful in reducing the number of extra devices. In our scheme, a beacon distributes its coordinates to its neighbors. If a node hears from three beacons (assuming the z coordinate to be fixed or to be calculated by a pressure sensor) it measures the distances in between and then applies lateration to estimate its coordinates. The distance can be estimated by Time of Arrival (ToA) assuming that the nodes are synchronized. Once the node is localized, it starts to distribute its coordinates to its neighbors (i.e. it acts as a new beacon).

Unfortunatly the inevitable errors in the distance measurements propagate and amplify through this distributed localization protocol. Measurement errors are due to several causes: i) the approximate speed of sound used in calculations, ii) the localization error in the first set of beacons, iii) estimation of the ToA has errors due to environmental noise (reflections, multipath, etc.) [37].

We study the *qualitative behavior* of the overall error as a function of the distance between a localized node and the set of initial beacons. We define the localization error of each node as follows:

- Let B be the set of initial beacons, we neglet the error of the beacons that are capable of autonomous localization. Thus, we have $e(b) = 0,\ \forall b \in B$.
- Let u be a node, and N_u be the set of localized neighbours of u that sent a message to u. If $|N_u| < 3$ node u cannot be localized, in the other case, consider the three nodes $n_1, n_2, n_3 \in N_u$ having minimum error. The error of u is defined as $e(u) = \frac{1}{3}(e(n_1) + e(n_2) + e(n_3)) + 1$.

This measure of error is the sum of the length of the minimum hop paths between a node and three nodes in B. We study how the number of localized nodes and the localization error is affected by varying the density of the initial set of beacons.

V. Simulations

A. Simulation Settings

The simulations use an underwater propagation model, implemented in Qualnet 3.9.5. The physical layer uses acoustic signals [38], [39]. At MAC layer we use CSMA. The speed of sound in water varies with water depth, salinity and temperature. In simulations, we use a speed of sound of 1513.74m/s. The transmission power was set to allow a communication range of 1000m. In addition, we had a constant shadowing effect with mean 2.0 dB. For each simulation experiment, we performed 10 runs with different initial deployment of nodes in the same area. The results presented are the averages over these 10 runs of simulation.

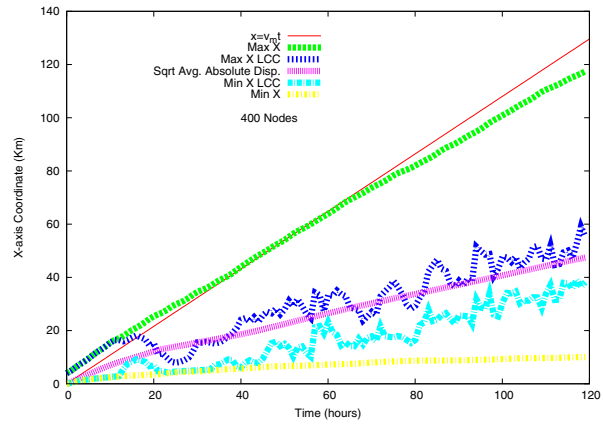

Fig. 4. Bounding box of the whole network, bounding box of $LCC(t)$, square root of absolute dispersion $A(t, t_0)$ and $x = v_m t$. Number of sensors $N = 400$.

B. Mobility Model and Network Connectivity

In this section we study the evolution of connectivity over time. Figure 4 represents the graphs of $x^G_{min}(t)$, $x^G_{max}(t)$, i.e. the bounding box of the whole network, and $x^{lcc}_{min}(t)$, $x^{lcc}_{max}(t)$, the bounding box of the largest connected component. The analysis of these functions show the movement of the whole network and of nodes belonging to the LCC with respect to time. The same plot contains the graph of the square root of absolute dispersion $A(t, t_0)$, and the trajectory $x = v_m t$, where $v_m = 0.3$m/s is the peak velocity in the jet (see Section II). The plot shows the movement of nodes along the x-axis in a period of 5 days.

Rigth after deployment, the network is connected, and clearly $x^G_{min}(t) = x^{lcc}_{min}(t)$ and $x^G_{max}(t) = x^{lcc}_{max}(t)$. Function $x^G_{max}(t)$ follows the same trajectory of function $x = v_m t$, meaning that some sensors are in the middle of the meandering current and move with velocity v_m. After some time, depending on the density of the network and the range of communication, the network becomes disconnected (which explains the drop in $x^{lcc}_{max}(t)$). A fraction of sensors continue to move with velocity v_m, determining the value of the maximum for the bonding box of the whole network ($x^G_{max}(t) \sim v_m t$), while a fraction of them remains trapped in the vortices determining the minimum of the bounding box of the whole network ($x^G_{min}(t)$). Nodes belonging to set LCC move with an average velocity smaller than v_m; this slow-down depends on the fact that the many sensors spend a significant part of their time circulating around in a vortex. Figure 5 represents the same information of Figure 4 in log-log scale. This figure shows more clearly the change in the velocity, before and after the network becomes disconnected.

The width of the bounding box of the whole network, i.e. the difference $x^G_{max}(t) - x^G_{min}(t)$ increases with time since nodes spread along all the domain. The bounding box of LCC remains smaller than the overall bounding box because the difference between the velocities of sensors in LCC cannot be

Authorized licensed use limited to: UNIVERSITY OF LECCE. Downloaded on February 27,2010 at 15:07:02 EST from IEEE Xplore. Restrictions apply.

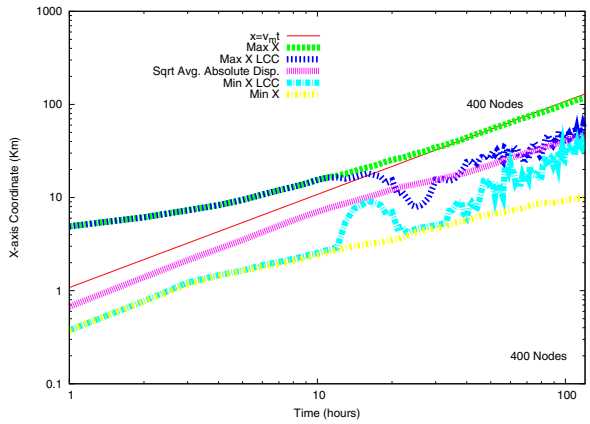

Fig. 5. Bounding box of the whole network, bounding box of $LCC(t)$, absolute dispersion (square root of) $A(t, t_0)$ and $x = v_m t$. Number of sensors $N = 400$. Log-Log scale.

too high, i.e. if a sensor in LCC moves with a velocity much lower or much higher than the remaining sensors, with high probability it will lose the connectivity with nodes in LCC, due to the limited communication range.

From Figure 4 we can state that the curve of the absolute dispersion follows the curve of $x^{lcc}_{max}(t)$. Thus the absolute dispersion: 1) is a good measure of the average velocity of nodes belonging to LCC; 2) is insensitive to the effect of nodes that move, respectivelly, too fast (in the center of the current) or too slow (in vortices) with respect to the majority of other nodes.

We observe that the number of deployed sensors is insufficient to guaranteed the connectivity if they were uniformly ditributed over the domain. Thus, as the transport due to the water currents spreads them apart we expect the network to be partitioned in several disconnected components.

In Figure 6 we plot the size of the LCC for a network of $N = 800$ and $N = 400$ sensors. In both cases the network stays connected for about 15 hours. After the disconnection the size of the LCC drops abruptly. In the high density case ($N = 800$) we observe sporadic jumps of the size of LCC from over $80\%N$ to about $40\%N$ and back to $80\%N$. They are the result of the interaction of LCC with vortices. Occasionally a consistent fraction of LCC is captured in a vortex, and it slows-down while the remaining part follows the jet downstream and disconnects from those in the vortex. Eventually most of the trapped nodes leave the vortex and enter the jet again. If the number of nodes is sufficiently high, they will be able to reconnect with LCC. As a consequence the average size of LCC is about $80\%N$ for the entire simulation. If the network is sparse ($N = 400$) the size of LCC decreases significantly with time. The decrease is not monotonous because some partial reconnections are still present.

The vortex permeability to sensors is affected by the choice of the parameters of the mobility model as we discussed in Section II. A detailed study of the impact of vortex permeability to network connectivity is left as a future work.

In Section III we relate the waiting time between different deployment rounds (ΔT) with the time (T_{ev} hereafter) required by sensors deployed in the first round to move out from the deployment area. To be sure that the nodes of the second deployment round are connected with those of the first one, we would like to choose T_{ev} in such a way that some nodes are still in the deployment region at the time of the second deployment.

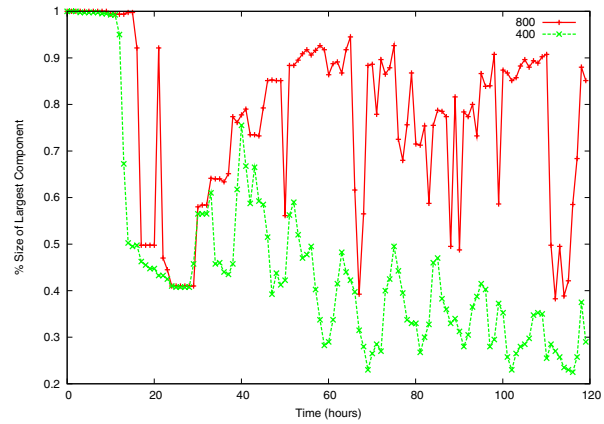

Fig. 6. Number of nodes in $LCC(t)$.

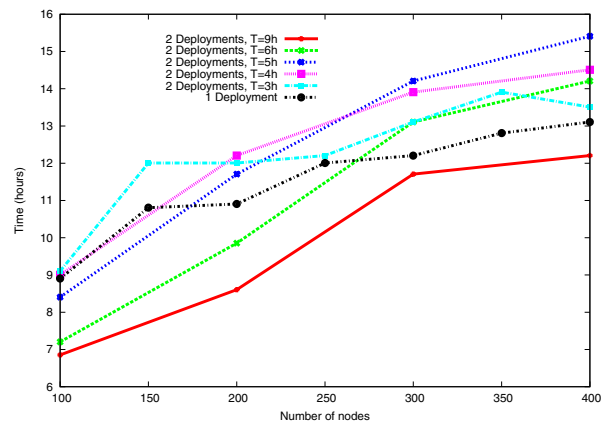

Fig. 7. Connectivity: first time when the size of the largest connected component drops below $90\%N$. Deployment with 1 or 2 rounds, and different values of ΔT.

We use the absolute dispersion as a measure of the average displacement of the LCC. Figure 5 shows that $A^2(t, t_0)$ is a power law, i.e. $A^2(t, t_0) \sim t^\alpha$. By least square fitting we obtain $\alpha \sim 1.7$. Note that this does not depend on N or R_c or other network parameters but is a characteristic of the mobility model. Since the deployment area has width equal to 4km, we have: $\sqrt{T_{ev}^{1.7}} = 4000$ which gives $T_{ev} = 4.8$.

The first drop in $x^{lcc}_{max}(t)$ corresponds to the first time of network disconnection. This time is a function of the number of nodes (density of the network), the communication range, and the meandering jet velocity. We study, in particular the first time when the number of sensors in LCC becomes less than $90\%N$ (T^{90}_{conn}), i.e. we measure the *lifetime* of the network with this value. In Figure 7 we plot T^{90}_{conn} for different values of N. For a fixed value of N we consider 1-round and 2-

Authorized licensed use limited to: UNIVERSITY OF LECCE. Downloaded on February 27,2010 at 15:07:02 EST from IEEE Xplore. Restrictions apply.

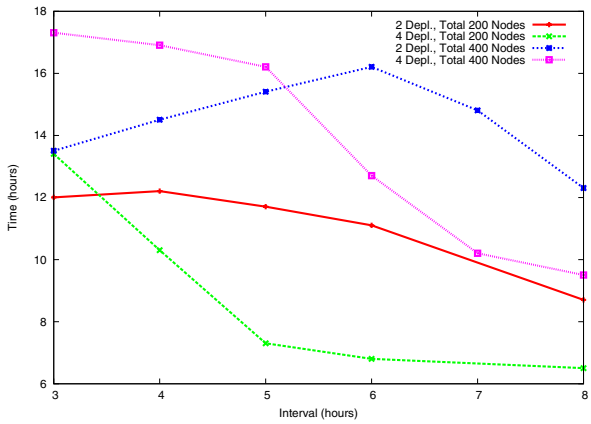

Fig. 8. Connectivity: first time when the size of the largest connected component drops below $90\%N$

round deployment, in the case of 2-round, we deploy $N/2$ nodes at $T = 0$ and the remaining $N/2$ at time $T = \Delta T$ with varying ΔT.

With a single deployment, the value of T^{90}_{conn} is in the range $[9 - 13]$h and it is clearly an increasing function of N. With two deployment rounds, if $\Delta T = 3$h or 4h, the value of T^{90}_{conn} increases, and in some case, like for large network ($N = 800$), it is 20% larger than the corresponding value using a single deployment.

If the value of ΔT is too high ($\Delta T = 9$h) the value of T^{90}_{conn} is always smaller than the corresponding value for a single deployment, since nodes in the second round are not able to catch the nodes of the first round.

In Figure 8, we study the impact of different values of ΔT in the case of 2 or 4 rounds of deployment, as before N is the total number of nodes, we consider $N = 200, 400$. In each round of deployment, if k is the number of rounds, N/k nodes are deployed uniformly in the region $[0, 4] \times [-2, 2]$km.

In the case of $N = 200$ and $\Delta T > 3$h increasing the number of deployment rounds does not improve T^{90}_{conn}. Because, with 3 deployments, the number of nodes in each round is only 50. This low value yields a disconnected network with high probability just after deployment. In the case of $N = 400$ and 2 deployments, T^{90}_{conn} increases with increasing value of ΔT up to $\Delta T = 6$h. Note that increasing the number of deployment rounds decrease the optimal value of ΔT since in each round we deploy less nodes.

C. Mobility model and Network Coverage

In this Section we report the simulation outcomes for the measures of coverage defined in Section III-B. Nodes are uniformly distributed in the deployment area and they disperse on the larger domain after deployment following the ocean current. In the simulation we use a disk model for the sensing area, with a sensing range equal to $R_s = 0.5$km for each node.

Figure 9 shows the impact of nodes movement on the *coverage area*, for networks with an increasing number of nodes. The dispersion of nodes from the deployment area towards the overall domain increases the area covered by the network.

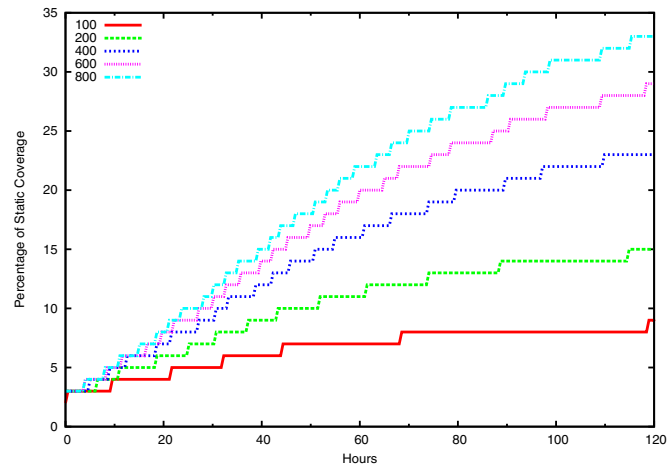

Fig. 9. Area Coverage of the network as percentage of the domain area. The domain is D=[0,80]x[-4,4]. Single deployment.

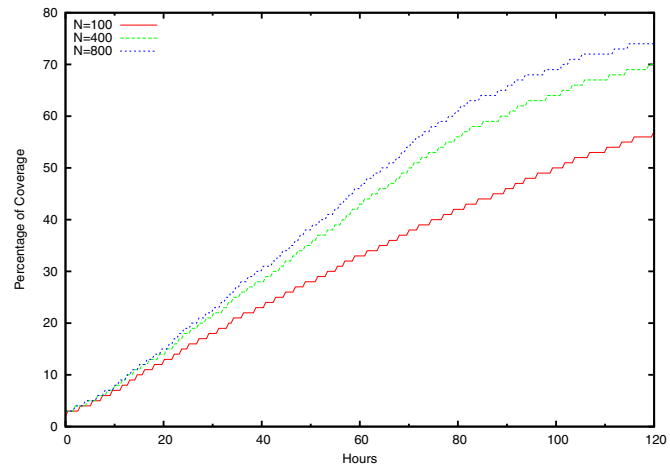

Fig. 10. Coverage over a time-interval of the network as percentage of the domain area. Single deployment.

The maximum area coverage is in any case only a fraction of the overall domain area. In Figure 10 we observe coverage area over time, i.e. for a given time t, the plot represents the fraction of the area of the domain, that has been covered at least one time in the interval $[0, t)$. We see from the plot, that mobility increases this "dynamic" coverage. It also increases with increasing network density as expected. In the case of multiple deployments, the choice of different number of rounds or different value of ΔT has a small effect on the 1-coverage. In both cases the area covered by nodes deployed starting from the second round is only a small fraction of the area covered by the initially deployed nodes.

D. Simulation results for Localization

In this section, we study the percentage of localized nodes and the localization error under varying percentage of beacons. The results show the average computed over four different simulation runs each with randomly selected initial set of beacons.

In Figure 11 we evaluate the progress of localization error for five days, for 800 nodes. On the first day (the left-hand side

Authorized licensed use limited to: UNIVERSITY OF LECCE. Downloaded on February 27,2010 at 15:07:02 EST from IEEE Xplore. Restrictions apply.

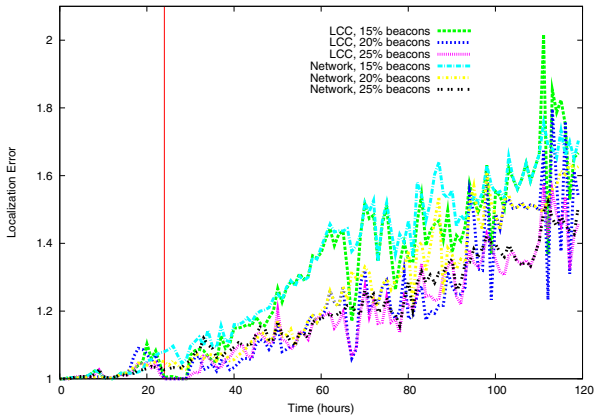

Fig. 11. Average of the localization error over time of the entire network and of the LCC, with $N = 800$, and number of beacons equals to $15\%, 20\%, 25\%$ of N.

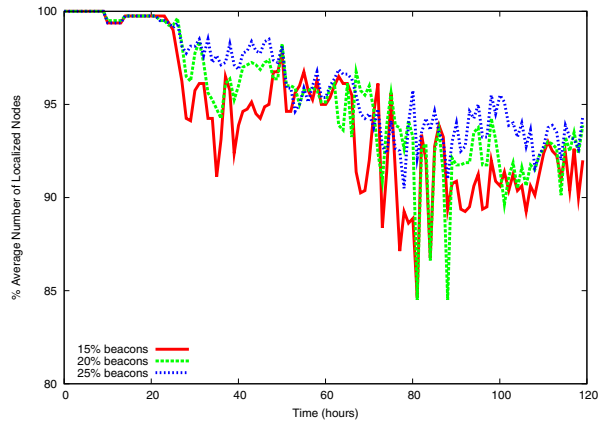

Fig. 12. Average percentage of localized nodes over time. Number of deployed nodes $N = 800$, and number of beacons equals to $15\%, 20\%, 25\%$ of N.

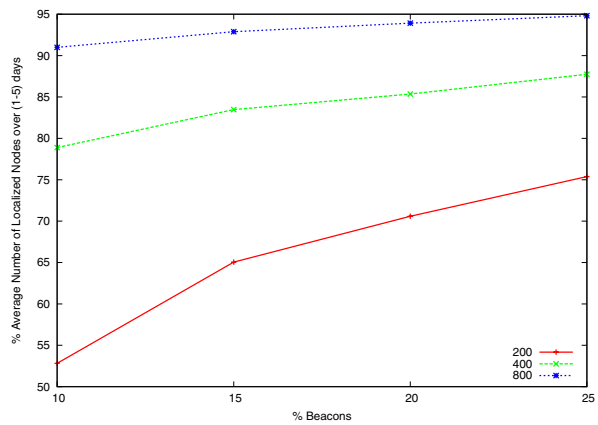

Fig. 13. Average number of localized nodes, with an increasing number of initial beacons.

of the vertical line), localization error is almost 1 which is the minimum error defined in Section IV. After the first day nodes start to get dispersed and the localization error increases. For the worst case with 15% beacons, there are at most 2 hops between the nodes and the beacons.

In Figure 12 we give the percentage of localized nodes versus simulation time for varying beacon percentages. On the first day, the network is connected and all the nodes are able to do localization. As the time evolves some nodes stay within the jet and some drift away inside the vortices. Majority of nodes stay in the jet, forming the LCC, and they get localization information always (all the nodes in LCC are localized). Other nodes that are captured by the vortices get disconnected from LCC and they have less chance to hear from three beacons. This figure resembles Fig. 6, i.e. there are oscillations of the number of localized nodes of high amplitude. This phenomenon has been already discussed when we studied the evolution of the size of LCC. In fact, both are related, since when sensors move out from the LCC the number of unlocalized nodes suddenly increase, while if they join the LCC it suddenly decreases. If the network is sufficiently dense, as the case in the figure, sensors exiting from the vortices join again the LCC and get once again localized. In the case of localization, the oscillations are smaller since even when a group of nodes move out of LCC there is a probability that this group includes three beacons, a sufficient condition to get localized, but the probability that this event occurs is not high.

Figure 13 shows the number of localized nodes for the entire network. We give results for 200, 400, 800 nodes. The results are averaged over time between days 2-5. We discard the first day of deployment. This figure shows only the analysis of the entire network, because as explained, localization for LCC has 100% success since there are enough number of beacons. The figure shows that the percentage of localized node in a sufficiently dense network is above 80% and it increases with an increasing number of initial beacons.

In Figure 14 we give the average localization error for varying beacon percentages for 200, 400 and 800 nodes. Here, by increasing the percentage of beacons the error converges to the minimum value, 1, i.e. most of the nodes hear directly from beacons, and the localization error remains bounded. The error decreases with increasing number of beacons since the number of nodes directly hearing fron the beacons increases. Since the number of hops is the direct measure for the error in our scheme, we state that the error decreases in a densely deployed network.

VI. Conclusion

In this paper, we introduced the Meandering Current Mobility model (MCM), for underwater mobile acoustic sensor networks. To the best of our knowledge this is the first physically-inspired mobility model used in the analysis of mobile underwater sensor networks. We started an analysis of the impact that the MCM model has on the network connectivity, coverage and on the error of a range-based localization scheme. We show that a multiple deployment process improves the connectivity lifetime of the sensor networks by studying how the waiting time between two rounds is related to the absolute dispersion of nodes. Our mobility model is dominated by a rather complicated, vortex-driven, process of disconnection and reconnection of portions of the network. This process is common to ocean flows. The present preliminary study

Authorized licensed use limited to: UNIVERSITY OF LECCE. Downloaded on February 27,2010 at 15:07:02 EST from IEEE Xplore. Restrictions apply.

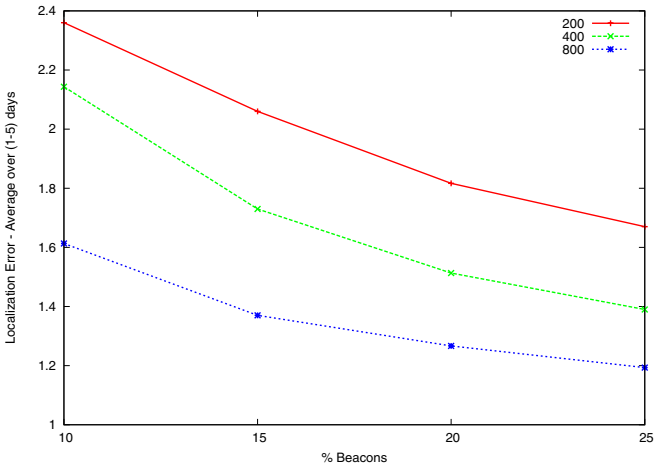

Fig. 14. Average of error in localization, with an increasing number of initial beacons.

intends to bring the attention of the network community on it, because it impacts on every aspect of networking, it is absent in conventional stochastic models and it could be exploited in the design of (delay-tolerant) routing algorithms. These topics will be the subject of future works.

REFERENCES

[1] I. F. Akyildiz, D. Pompili, and T. Melodia, "Underwater acoustic sensor networks: research challenges," *Ad Hoc Networks*, vol. 2, no. 3, pp. 257–279, March 2005.

[2] J. Partan, J. Kurose, and B. N. Levine, "A survey of practical issues in underwater networks," in *WUWNet'06*, Los Angeles, CA, USA, 2006, pp. 17–24.

[3] J. Kong, J. Cui, D. Wu, and M. Gerla, "Building underwater ad-hoc networks and sensor networks for large scale real-time aquatic applications," in *IEEE MILCOM*, Atlantic City, NJ, USA, 2005.

[4] I. Vasilescu, K. Kotay, D. Rus, M. Dunbabin, and P. Corke, "Data collection, storage, and retrieval with an underwater sensor network," in *SenSys'05*, San Diego, California, USA, 2005, pp. 154–165.

[5] A. Syed and J. Heidemann, "Time synchronization for high latency acoustic networks," in *Proc. of Infocom*, Barcelona, Spain, April 2006, pp. 1–12.

[6] V. Chandrasekhar, W. K. Seah, Y. S. Choo, and H. V. Ee, "Localization in underwater sensor networks: survey and challenges," in *WUWNet '06*, Los Angeles, CA, USA, 2006, pp. 33–40.

[7] D. Pompili and T. Melodia, "Three-dimensional routing in underwater acoustic sensor networks," in *PE-WASUN '05: Proc. of the 2nd ACM Int. workshop on Performance evaluation of wireless ad hoc, sensor, and ubiquitous networks*, Montreal, Quebec, Canada, 2005, pp. 214–221.

[8] P. Xie, J. Cui, and L. Lao, "Vbf: Vector-based forwarding protocol for underwater sensor networks," in *In Proc. of IFIP Networking'06*, Portugual, May 2006, pp. 1216–1221.

[9] N. Chirdchoo, W.-S. Soh, and K. C. Chua, "Aloha-based mac protocols with collision avoidance for underwater acoustic networks," in *INFOCOM 2007*, Anchorage, Alaska, USA, May 2007, pp. 2271–2275.

[10] D. Makhija, P. Kumaraswamy, and R. Roy, "Challenges and design of mac protocol for underwater acoustic sensor networks," in *4th International Symposium on Modeling and Optimization in Mobile, Ad Hoc and Wireless Networks*, Boston, Massachusetts, USA, 03-06 April 2006, pp. 1–6.

[11] E. Cayirci, H. Tezcan, Y. Dogan, and V. Coskun, "Wireless sensor networks for underwater surveillance systems," *Ad Hoc Networks*, vol. 4, no. 4, pp. 431–446, 2006.

[12] J. Heidemann, W. Ye, J. Wills, A. Syed, and Y. Li, "Research challenges and applications for underwater sensor networking," in *IEEE Wireless Communications and Networking Conference (WCNC)*, April 2006.

[13] S. Roy, P. Arabshahi, D. Rouseff, and W. Fox, "Wide area ocean networks: architecture and system design considerations," in *WUWNet'06*. Los Angeles, CA, USA: ACM Press, 2006, pp. 25–32.

[14] J. Jaffe and C. Schurgers, "Sensor networks of freely drifting autonomous underwater explorers," in *WUWNet'06*, Los Angeles, CA, USA, 2006, pp. 93–96.

[15] R. E. Davis, "Lagrangian ocean studies," *Annual Review of Fluid Mechanics*, vol. 23, pp. 43–64, 1991.

[16] W. Gould and J. Turton, "Argo – sounding the oceans," *Weather*, vol. 61, no. 1, pp. 17–21, 2006.

[17] J. C. Ohlmann, P. F. White, A. L. Sybrandy, and P. P. Niiler, "GPS-Cellular Drifter Technology for Coastal Ocean Observing Systems," *Journal of Atmospheric and Oceanic Technology*, vol. 22, pp. 1382–1388, 2005.

[18] C. Bettstetter, *Mobility Modeling, Connectivity, and Adaptive Clustering in Ad Hoc Networks*. Utz Verlag, 2004.

[19] C. Bettstetter, H. Hartenstein, and X. Perez-Costa, "Stochastic properties of the random waypoint mobility model," *Wireless Networks*, vol. 10, no. 5, pp. 555–567, 2004.

[20] J. Yoon, M. Liu, and B. Noble, "Random waypoint considered harmful," in *INFOCOM 2003*, 30 March-3 April 2003, pp. 1312–1321.

[21] E. Chassignet, H. Hurlburt, O. Smedstad, G. Halliwell, A. Wallcraft, E. Metzger, B. Blanton, C. Lozano, D. Rao, P. Hogan, and A. Srinivasan, "Generalized vertical coordinates for eddy-resolving global and coastal ocean forecasts," *Oceanography*, no. 19, pp. 20–31, 2006.

[22] J. Pedlosky, *Ocean Circulation Theory*. Heidelberg: Springer-Verlag, 1996.

[23] J. M. Ottino, *The Kinematics of Mixing: Stretching, Chaos, and Transport*, ser. Cambridge Texts in Applied Mathematics. Cambridge University Press, 1989, no. 3.

[24] R. M. Samelson and S. Wiggins, *Lagrangian Transport in Geophysical Jets and Waves. The Dynamical Systems Approach*, ser. Interdisciplinary Applied Mathematics. Springer-Verlag, 2006, no. 31.

[25] R. Davis, "Drifter observations of coastal surface currents during CODE: the method and descriptive view," *J. Geophys. Res.*, no. 90, pp. 4741–4755, 1985.

[26] A. Sybrandy and P. Niiler, "Woce/toga lagrangian drifter construction manual." San Diego, California, Scripps Institution of Oceanography, Tech. Rep., 1991, sIO REF 91/6, WOCE Report 63.

[27] T. Rossby, D. Dorson, and J. Fontaine, "The rafos system." *J. Atmos. Oceanic Tech.*, vol. 3, no. 4, pp. 672–679, 1986.

[28] A. S. Bower, "A simple kinematic mechanism for mixing fluid parcels across a meandering jet," *J. Phys. Ocean.*, vol. 21, no. 1, pp. 173–180, 1991.

[29] R. M. Samelson, "Fluid exchange across a meandering jet," *J. Phys. Ocean.*, vol. 22, no. 4, pp. 431–440, 1992.

[30] M. Cencini, G. Lacorata, A. Vulpiani, and E. Zambianchi, "Mixing in a meandering jet: a markovian approximation," *J. Phys. Ocean.*, vol. 29, no. 10, pp. 2578–2594, 1999.

[31] A. Provenzale, "Transport by coherent barotropic vortices," *Annual Rev. Fluid Mech.*, vol. 31, pp. 55–93, 1999.

[32] K. Fall, "A delay-tolerant network architecture for challenged internets," in *SIGCOMM '03*, Karlsruhe, Germany, 2003, pp. 27–34.

[33] B. Liu, P. Brass, O. Dousse, P. Nain, and D. Towsley, "Mobility improves coverage of sensor networks," in *MobiHoc '05*, Urbana-Champaign, IL, USA, 2005, pp. 300–308.

[34] A. K. Othman, A. E. Adams, and C. C. Tsimenidis, "Node discovery protocol and localization for distributed underwater acoustic networks," in *AICT-ICIW '06: Proc. of the Adv. Int. Conf. on Telecommunications and Int. Conf. on Internet and Web Applications and Services*, Washington, DC, USA, 2006, p. 93.

[35] Z. Zhou, J. Cui, and S. Zhou, "Localization for Large-Scale Underwater Sensor Networks," in *UCONN CSE Technical Report:UbiNet-TR06-04*, 2006.

[36] M. Erol, L. Vieira, and M. Gerla, "Localization with divenrise (dnr) beacons for underwater sensor networks," in *to be presented in WUWnet'07*, 2007.

[37] L. Collin, S. Azou, K. Yao, and G. Burel, "On spatial uncertainty in a surface long baseline positioning system," in *Proceedings of the Fifth European Conference on Underwater Acoustics, ECUA 2000*, Lyon, France, 2000, pp. 607–612.

[38] J. P. E.M. Sozer, M. Stojanovic, "Underwater acoustic networks," *IEEE Journal of Oceanic Engineering*, vol. 25, no. 1, pp. 72–83, 2000.

[39] M. Stojanovic, *Acoustic (underwater) communications*, J.G.Proakis, Ed. Wiley, 2003.

Authorized licensed use limited to: UNIVERSITY OF LECCE. Downloaded on February 27,2010 at 15:07:02 EST from IEEE Xplore. Restrictions apply.